Nonhuman Primate Eyes Display Variable Growth and Aging Rates in Alignment With Human Eyes

Ying Xue,[1] Yingxue Cao,[1] Shuxin Fan,[1] Mingming Xu,[1] Ziqi Yang,[1] Lingli Zhou,[1,2] Le Shi,[1] Lechun Ou,[1] Yuying Li,[1] Wenjie Qing,[1] Zhicheng Zou,[1] Fuxiang Mao,[1] Ningli Wang,[3] Elia J. Duh,[2] Wei Yi,[1] and Xialin Liu[1]

[1]State Key Laboratory of Ophthalmology, Zhongshan Ophthalmic Center, Sun Yat-Sen University, Guangdong Provincial Key Laboratory of Ophthalmology and Visual Science, Guangzhou, China
[2]Department of Ophthalmology, Johns Hopkins School of Medicine, Baltimore, MD, United States
[3]Beijing Tongren Hospital, Capital Medical University, Beijing Institute of Ophthalmology, Beijing, China

Correspondence: Wei Yi, State Key Laboratory of Ophthalmology, Zhongshan Ophthalmic Center, Sun Yat-Sen University, Guangdong Provincial Key Laboratory of Ophthalmology and Visual Science, 510060 Guangzhou, China; yiwei7@mail.sysu.edu.cn.
Xialin Liu, State Key Laboratory of Ophthalmology, Zhongshan Ophthalmic Center, Sun Yat-Sen University, Guangdong Provincial Key Laboratory of Ophthalmology and Visual Science, 510060 Guangzhou, China; liuxl28@mail.sysu.edu.cn.

YX and YC contributed equally to this work.

Received: March 21, 2023
Accepted: July 25, 2023
Published: August 17, 2023

Citation: Xue Y, Cao Y, Fan S, et al. Nonhuman primate eyes display variable growth and aging rates in alignment with human eyes. *Invest Ophthalmol Vis Sci.* 2023;64(11):23. https://doi.org/10.1167/iovs.64.11.23

Purpose. To assess age-related biometric changes of the eye in nonhuman primates (NHPs), to and decipher the growth and aging rates and their comparability with humans.

Methods. Ocular anatomic measurements were performed on 341 *macaca fascicularis* aged 0.5 to 23 years via multimodal approaches including IOLMaster 700. Linear or polynomial regression models were simulated to determine the best fitted age-related function. The metrics were compared with human equivalents in published reports.

Results. Macaques exhibited a postnatal eye growth pattern similar to humans, characterized by continuous eye extension coordinated with dramatic reshaping of the lens but not the cornea. The age-related growth of lens thickness (LT), anterior chamber depth (ACD), and axis length (AL) exhibited nonlinear and bipolar patterns. The inflection points were 10 to 12 years old for LT and ACD and 13 to 15 years old for AL in macaques, which were comparable in chronological age at a ratio of ~1: ratio with that in humans. In contrast, the speed of aging, including the increase in lens density and the decrease in retinal nerve fiber layer thickness, was comparable in relative age at a ratio of ~1:3 according to the differences in lifespan between macaques and humans. Lens density was a robust indicator for the aging process.

Conclusions. Macaque eyes recapitulated the age-related process of human eyes to varying extents with different growth and aging rates. Chronological age or relative age should be considered in different scenarios when macaques are included in preclinical studies.

Keywords: ocular biometrics, nonhuman primate, development, ocular, aging, IOLmaster 700

Age plays a critical role in organ growth and the progression of many diseases.[1] For the human visual system, age contributes to the maturation of ocular structures and emmetropization during growth as well as the development and progression of the major causes of age-related blindness.[2,3] Nonhuman primate macaques, including *macaca mulatta* (rhesus macaque) and *macaca fascicularis* (crab-eating macaque), have been used as experimental animal models for decades.[4] Unlike common animal models such as fish and rodents, macaques share with humans a highly developed visual system, including many primate-specific structures such as the macula and elliptical lens, which make these animals indispensable models for ophthalmology and vision research.[2,5,6] However, the high genetic diversity, long lifespan, and high cost of macaque models relative to other animal models have limited the systematic understanding of age-induced ocular biometric changes in these animals. For example, various studies have reported that lens thickness (LT) in macaques increased, decreased, or did not change with age.[7–11] How the growth and aging of the eye globe and ocular components, including the lens and cornea, are coordinated in macaques remains to be illustrated.

Generally, the alignment of biological processes across species with different lifespans is based on the concept of the lifespan ratio.[12] The ratio is ~1:3 when comparing the relative age of monkeys and humans, in which ~20 monkey years are equivalent to 60 human years.[13] However, emerging evidence shows that the pace of growth and decline vary among different tissues, even within one species.[14] In humans, corneal diameter and curvature, measured as white to white (WTW) and curvature radius (CR), generally reach adult values during the first year of life.[2] In contrast, the lens undergoes a significant change in shape with a remarkable decrease in sagittal LT in the first 10 years of life and then

an increase thereafter.[15–17] Additionally, the growth in axial length (AL) of the human globe generally lasts up to age 25.[2,15] The age-related degeneration of retinal nerve fiber layer is relatively minor, but the aging of the crystalline lens is fast so that a high prevalence of cataracts is observed in the elderly human population.[18] The heterogeneity of age-related changes in eyes raises the question of how the growth and aging process of macaque eyes can be aligned with humans. An accurate and systematic comparison of the age-related changes between macaque and human eye components is crucial for developing appropriate preclinical primate ophthalmic models and understanding the nature of our own species.

Recent advances in ocular imaging techniques allow accurate biometric measurements and high-resolution structural visualization in clinics.[19] For example, a new-generation optical instrument, the IOLMaster 700, provides a swept-source optical coherence tomography (ss-OCT) image-based measurement to view and quantify the complete longitudinal section of the eye in vivo,[20] making it possible to accurately compare the age-related changes between macaque and human ocular components. In this study, through systematic ocular biometric measurements of postnatal macaques aged 0.5 to 23 years with advanced multimodal imaging techniques and various model simulations, we sought to evaluate age-related ocular biometric changes and compare age-related growth and aging between macaque and human eyes.

Methods

Animals

All crab-eating macaques (*macaca fascicularis*) were from Huazhen Biotechnology Co., Ltd, Guangzhou, China. The animals were born and maintained at ~ 26°C and 40% to 70% room humidity on a 12-hour/12-hour light/dark cycle at the Huazhen Laboratory Animal Breeding Centre. The animals had no surgical history. All animal procedures adhered to the ARVO Statement for the Use of Animals in Ophthalmic and Vision Research and were approved and monitored by the Institutional Animal Care and Use Committee of Zhongshan Ophthalmic Center (no. W2021023).

Ocular Biometry

Animals were monitored by a trained technician and a veterinarian at all times. The animals were sedated with an intramuscular injection of Zoletil 50 (VIRBAC S.A.) (4 mg/kg) and topical application of proparacaine HCl (Alcaine, 0.5%; Alcon Laboratories, Geneva, Switzerland). Intraocular pressure (IOP) was measured using a Tonovet tonometer (Icare Finland Oy, Vantaa, Finland). AL, CR, WTW, central corneal thickness (CCT), anterior chamber depth (ACD), LT, and vitreous chamber depth (VCD) were measured using an IOLMaster 700 (Carl Zeiss Meditec AG, Jena, Germany). According to the measurements obtained with the IOLMaster 700, the ACD value is equal to the sum of CCT and aqueous humor depth, and the AL value corresponds to "ACD + LT + VCD." We observed that the measurements of WTW by IOLMaster 700 were inaccurate because of the interference caused by the pigmentation of the conjunctiva of macaque eyes, making autonomous recognition of the corneal limbus challenging. However, the pupillary margin was accurately recognized. To address this issue, we used Photoshop (CS6; Adobe Systems Software, Ireland Ltd) to measure the relative length of WTW and pupil and adjusted the WTW value based on the pupil diameter measured by IOLMaster700 (Supplementary Fig. S1). We excluded low-quality ophthalmic data from eyes with incorrect eye position because of anesthesia and eyes with obvious ocular trauma history.

Slit-Lamp Imaging, Color Fundus Photography, and OCT Tomography

Pupils were dilated with 0.5% tropicamide. Lenses were examined and imaged with slit-lamp biomicroscopy (SL-D701; Topcon, Tokyo, Japan). Color fundus photographs were obtained with a conventional flash fundus camera (TRC-NW8, Topcon Corporation). Spectral domain OCT was performed with Heidelberg HRA-OCT (Spectralis; Heidelberg Engineering GmbH, Heidelberg, Germany) according to the standard manufacturer's protocol. For the measurement of peripapillary RNFL, a glaucoma protocol with a single circular B-scan of 12° diameter was performed. Each B-scan consisted of 512 A-scans along a 3.4-mm diameter circular ring around the optic disk. The RNFL was automatically segmented using the Heidelberg HRA-OCT software, and any inaccuracies were manually calibrated by a masked technician. The original reads of peripapillary retinal nerve fiber layer thickness (RNFLT) were measured from the Heidelberg HRA-OCT software. Of note, the ocular biometry studies in the current study includes all the macaques that were examined, including some macaques that presented macular drusenoid deposits (>63 µm) within 2 disc diameters of the fovea in color fundus photographs and OCT examinations, which were considered as pathogenic drusen according to Age-Related Macular Degeneration PPP 2019 by the American Academy of Ophthalmology.[21]

Measurement of Lens Density

The density of the lens cortex (LC) and nucleus (LN) were calculated by open-source ImageJ software (National Institutes of Health, Bethesda, MD, USA). Images captured from the SS-OCT B-scans of the lens by IOLMaster 700 were exported to ImageJ. Mean signals from the squares of 20 × 20 pixels at a fixed distance in front of the eye in the image were calculated as the baseline value. Mean signals from the squares in the lens anterior cortex, the lens posterior cortex and the lens nucleus were calculated (Fig. 3A). We have observed that the B-scanning light waves sometimes induce a halo effect that interferes with the signal in the areas near the B-scan meridian on the image. To ensure accuracy and consistency between measurements, we have chosen symmetrical areas of the lens, precisely 10 pixels above and below the B-scan meridian. The densities of the lens cortex and nucleus were calculated by averaging the signals from the top and bottom target squares and then scaling them to the baseline value.

Statistical Analysis

Statistical computing and visualization were carried out using R (version 4.0.5) and the R packages ggpubr, ggpmisc and ggplot2. The correlations of age with all the continuous variables for each sex were visualized first with scatterplots. For the analysis of WTW and lens density, we selected one eye from each animal for manual measurement of the parameters, representing that animal as a single biological replicate. For AL, CCT, ACD, LT, VCD, IOP and RNFLT, we used the averaged binocular measurements of one animal as

a single biological replicate. Linear and polynomial regression analyses of age and each biometry variable were tested to develop model simulations of the age-related pattern. The adjusted R^2 values and P values were calculated for each model to determine which model achieved the best fit. The equations of the model with the best fit were obtained to calculate the inflection points of the simulated curve. The position of the inflection point was considered the turning age of maturation and maximum or minimum adult value. The speed of aging at defined ages was determined by calculating the derivative of the age-related equation.

Results

Animals

According to the time of reproductive debut and time of sexual maturity, macaques can be classified into infant, juvenile, subadult, adult, and geriatric stages.[22,23] To map the ocular changes in their lifespan, we acquired data from 341 crab-eating macaques with ages ranging from 0.5 to 23 years, covering all the postnatal stages of a macaque's lifecycle after weaning, as shown in Table 1 with respect to the age distribution.

Ocular Biometry and Regression Model Simulation

Ocular biometry, including IOP, AL, WTW, CR, CCT, ACD, LT, and VCD, was performed. To determine the best fitted function of age for the variables, we used linear regression and polynomial regression models with increasing orders for simulation. Compared with a linear regression model, the second-order polynomial regression model could significantly improve the fitness of the age-related pattern for variables including IOP, AL, LT, ACD, CCT, and VCD and further increase the order only slightly or increase the simulation power, indicated as R^2 values and P values (Fig. 1A). We thus used second-order polynomial regression models for these variables. However, WTW and CR failed to show a significant

Table 1. Age Distribution of Crab-Eating Macaques Examined in This Study

Stage	Stage Define	Number (Male/Female)	Age Range (Y)	Age (Y), Mean ± SD
Infant	0–1.5 y	41 (21/20)	0.7–1.2	0.9 ± 0.1
Juvenile	1.5–4 y	94 (45/49)	1.6–3.9	2.7 ± 0.8
Sub-adult	4–9 y	116 (56/60)	4.0–8.8	5.2 ± 1.4
Adult	9–20 y	78 (34/44)	10.2–19.9	16.5 ± 3.2
Geriatric	20–25 y	12 (10/2)	20.1–22.40	21.0 ± 0.7
Total		341 (166/175)	0.7–22.4	7.2 ± 6.4

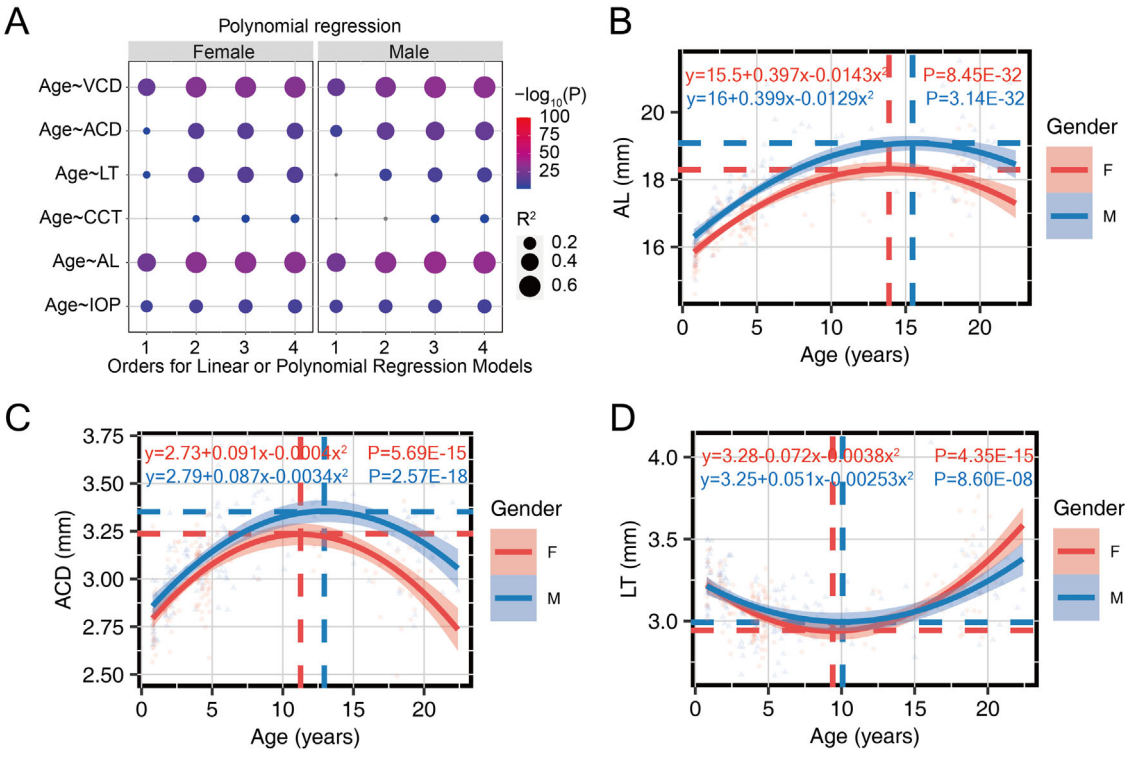

Figure 1. The ocular components displayed biphasic age-related patterns. (**A**) The power (R^2) and P value for age-related patterns of multiple variables simulated with the linear regression model (first order) or second-, third-, or fourth-order polynomial regression models. (**B, C**) The best fitted age-related growth patterns of (**B**) AL and (**C**) ACD showed an inverted U shape. (**D**) The best fitted age-related pattern of LT showed a U shape. The *dashed lines* indicate the X and Y positions of the inflection point. The second-order polynomial regression formula for each variable as a function of age, and the P values were provided. *Red* for females and *blue* for males.

Investigative Ophthalmology & Visual Science

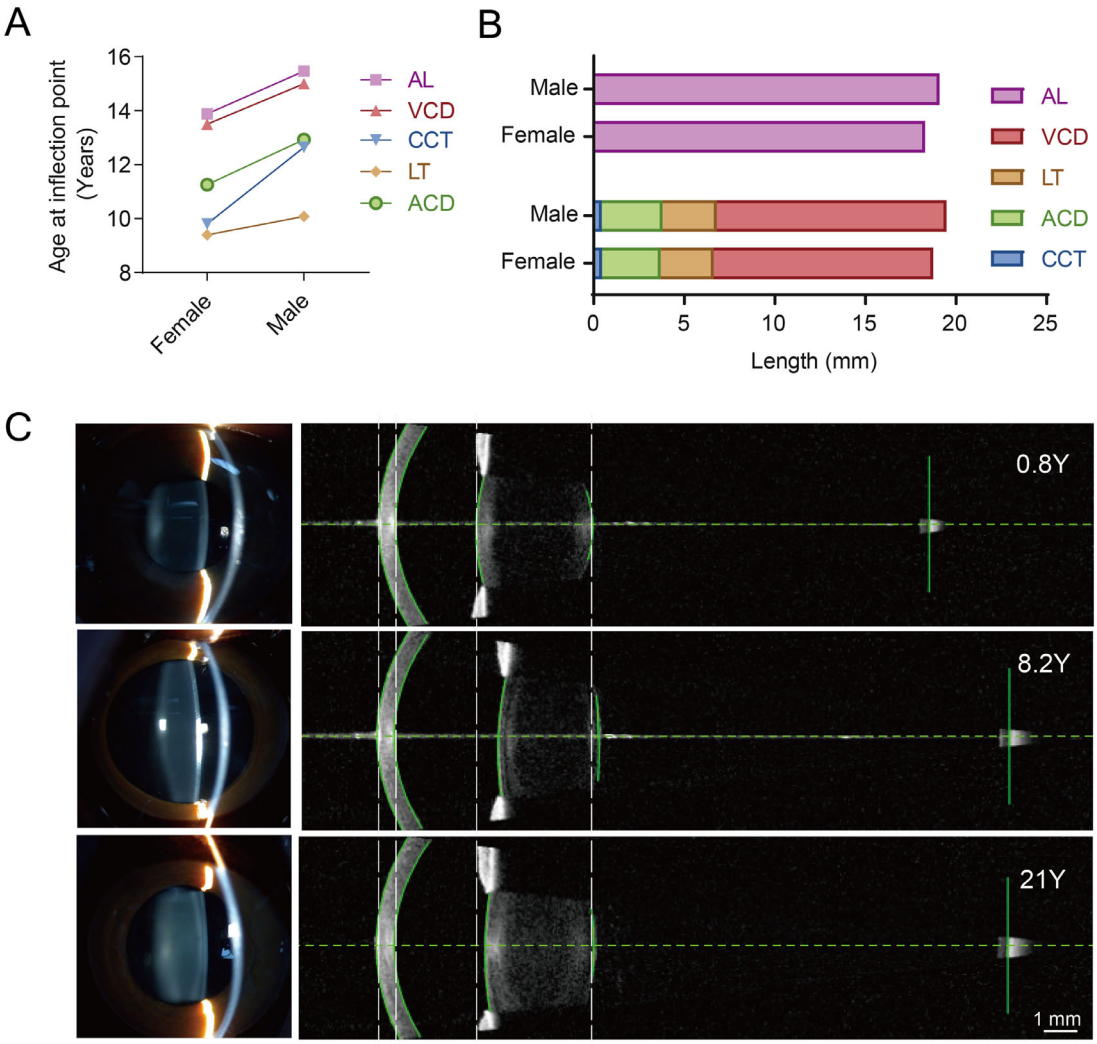

Figure 2. The growth metrics of the ocular components in macaques. (**A**) The ages at the inflection point for LT, ACD, and CCT were older than those for AL and VCD and were older in males than females for all variables. (**B**) The length of eye components at the inflection point in males and females. (**C**) Representative images captured from slit-lamp photography (*left*) and from IOLMaster (*right*) for animals of different ages. From top to bottom: 0.8 years, male; 8.2 years, male and 21 years, male.

correlation with age in all the models, suggesting no discernible trend in the measured lifecycle (Supplementary Figs. S2A, S2B).

The changes in AL, ACD, CCT, VCD, and IOP with age showed typical inverted U shapes, which indicated a fast increase at an early postnatal age, followed by a more gradual increase until the peak and a gradual decrease later in life (Figs. 1B, 1C, Supplementary Figs. S3A–C). In contrast, the age-related change in LT exhibited a U shape (Fig. 1D), where LT continued decreasing with age and then increased later in life. The simulated equations were calculated to provide reference data for macaques at any age. The inflection points for the first half of these trends were considered as the growth milestones for the ocular components, and their X and Y axial positions were calculated as the turning age for maturation and extreme value for each variable, respectively.

The mature ages for the ocular components in the anterior segments were generally younger than those for VCD and AL in both sexes (Fig. 2A). Compared with females, males showed older mature ages (Fig. 2A) and longer eyes because of slightly deeper ACD and VCD (Fig. 2B). Apparent changes in ocular biometry can be observed in the representative SS-OCT images from the IOL master among individuals at various ages (Fig. 2C).

Alignment of Growth Metrics Between Macaques and Humans

Next, we compared the growth metrics with the human equivalents from previous epidemiological studies, meta-analyses, and reviews[2,15–17,24–28] and aligned the growth milestones according to the lifespan ratio (1:3) between macaques and humans (Table 2). The adult values were all smaller in macaques than in humans, except for ACD, suggesting that macaque eyes are generally smaller than human eyes but have relatively deeper anterior chambers when scaled to their eye size. The growth stage refers to the period from birth to the inflection point, at which ocular

Investigative Ophthalmology & Visual Science

Table 2. Alignment of the Age-Related Metrics Between Macaques and Humans

	Mean (SD) in Adult		Age at Inflection Point (Y)		
			Chronologic Age		Relative Age
	H.S.	M.F.*	H.S.	M.F.	M.F.†
AL	23.49 mm (1.35)[28]		~20–25[2,15]		
All		18.40 mm (1.03)		14.96	44.88
F		18.04 mm (0.86)		13.88	41.64
M		18.75 mm (1.05)		15.47	46.41
LT	4.37 mm (0.43)[28]		~10[2,15–17]		
All		3.19 mm (0.25)		9.66	28.98
F		3.20 mm (0.25)		9.40	28.2
M		3.18 mm (0.25)		10.08	30.24
ACD	3.10 mm (0.47)[28]		~12[24,25,28]		
All		3.14 mm (0.22)		12.23	36.69
F		3.06 mm (0.21)		11.26	33.78
M		3.21 mm (0.21)		12.93	38.79
CCT	544 µm (38)[28]		~11[26,27]		
All		445 µm (29)		10.73	32.19
F		440 µm (26)		9.81	29.43
M		449 µm (30)		12.64	37.92
CR	7.69 mm (0.28)[28]		~1[2,15]	NA‡	NA‡
All		5.77 mm (0.17)			
F		5.72 mm (0.15)			
M		5.82 mm (0.18)			
WTW	11.80 mm (0.42)[28]		~1[2,15]	NA‡	NA‡
All		9.64 mm (0.36)			
F		9.49 mm (0.37)			
M		9.74 mm (0.32)			

M.F., macaca fascicularis; H.S., homo sapiens.
* Included data from macaques >9 years old.
† Relative age in macaques was calculated by multiplying the chronologic age in macaques by the ratio of 3:1 (average lifespan ratio between humans and macaques).
‡ No significant trend detected.

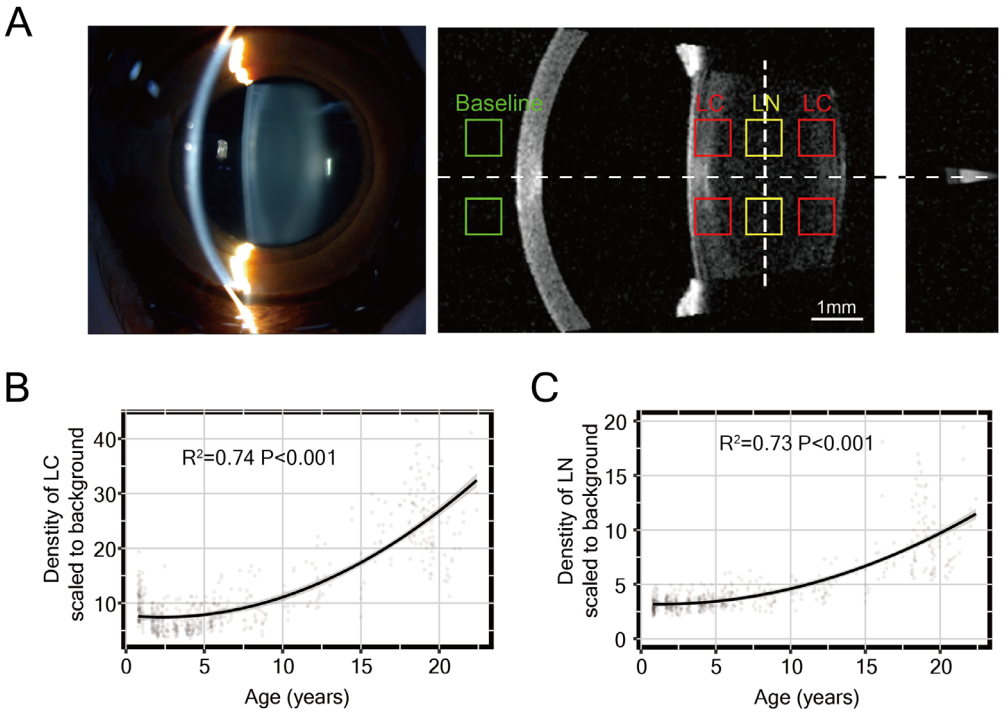

Figure 3. Lens opacity robustly increased with age in macaque eyes. (**A**) Schematic diagram of lens density measurement for ss-OCT image by IOL Master 700. The slit-lamp image of the same eye is shown on the left. The mean gray signal was measured from the nuclear area (*yellow squares*), cortex area (*red squares*), and baseline area (*green squares*). (**B, C**) The density of the nucleus (**B**) and cortex (**C**) of the lens showed an accelerated increase with age after approximately six years of age. The power (R^2) and P value are provided.

Investigative Ophthalmology & Visual Science

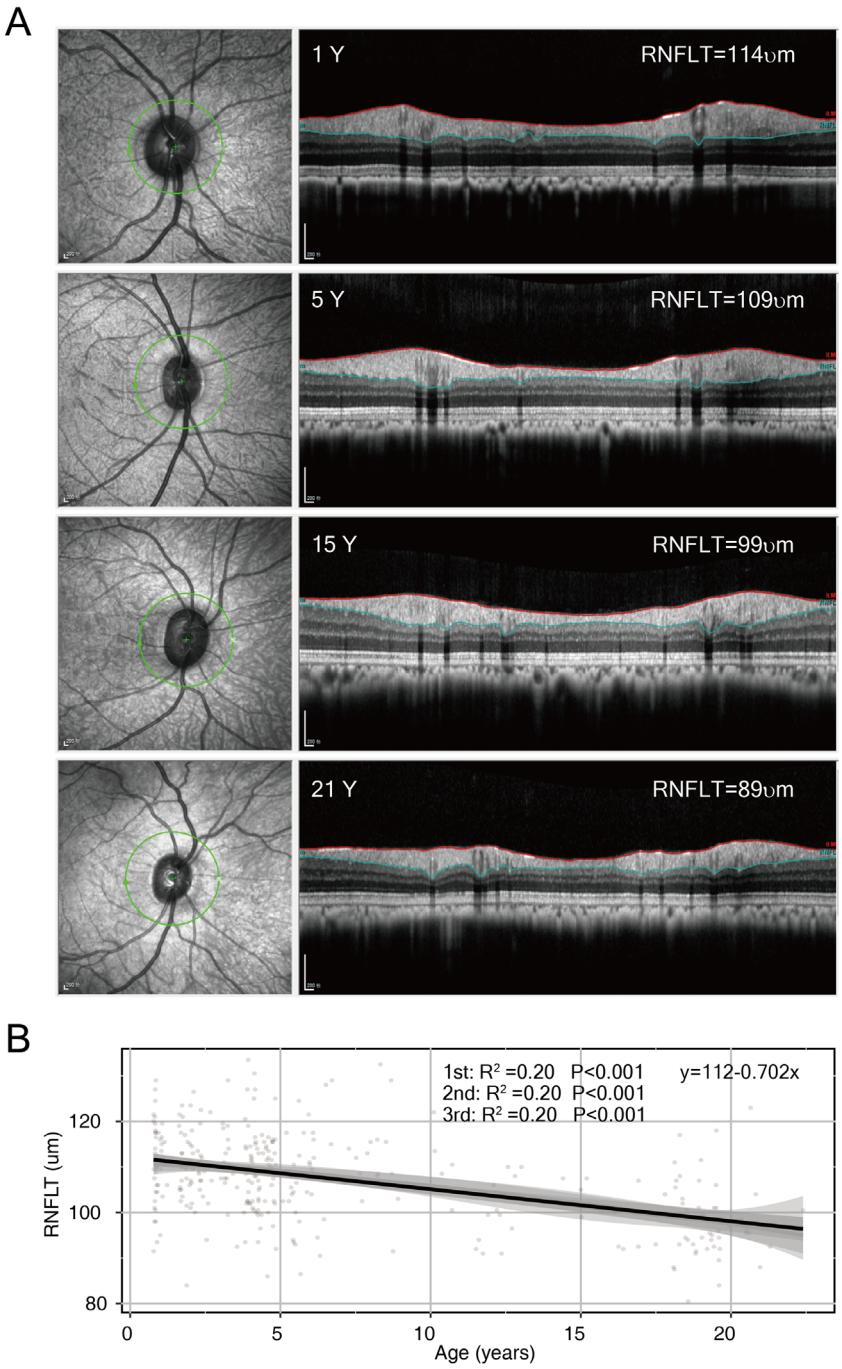

Figure 4. RNFLT showed a significant linear decrease trend with age in macaque eyes. (**A**) Representative OCT images from animals of different ages. From top to bottom: one year (male), five years (male), 15 years (male), and 21 years (male). (**B**) The correlation between RNFLT and age was analyzed using linear regression (first-order) or polynomial regression (second and third), both showing similar power. A formula fitted to linear regression was provided.

parameters reach their maximum or minimum values. The ages corresponding to the turning points were considered to determine the rate of growth for each ocular component. We found that in both macaques and humans, the postnatal eye growth patterns were conserved, exhibiting continuous axial growth of the eye globe years after birth that was coordinated with the reshaping of the lens but not the cornea. However, when comparing the speed of growth indicated by the turning age at the inflection point, we found that both species stopped lens thinning and anterior chamber deepening at approximately chronologic age 10. The extension of axial length was stabilized at approximately age 15 in macaques and approximately age 20 to 25 in humans. The turning points of these refraction components in macaques were similar to those in humans in chronological age by an ~1:1 ratio, whereas all were much older in relative age according to the 3:1 ratio.

Investigative Ophthalmology & Visual Science

Aging Speed of the Lens Between Macaques and Humans

During aging in humans, it is known that the crystalline lens increases opacity before the appearance of pathogenic cataracts, as quantified previously by various techniques.[29] Such quantitative evaluation of aging in the macaque lens has not previously been described, although cataracts have been reported in macaques.[30] We noticed that the signal in the lens area from images captured from IOLMaster 700 increased with age even when no clinically significant cataract was evident (Fig. 2C). We thus introduced objective quantification of the density of the LC and LN by measuring the signals from the LC and LN, respectively, from the ss-OCT images (Fig. 3A).

The quantitative results revealed that the densities of both LC and LN were strongly correlated ($R^2 > 0.7$) with age (Figs. 3B, 3C). The density of the lens for both LC and LN increased substantially after approximately six years of age. The quadratic increasing trend of quantitative lens density with age was reported in human populations starting at age 20,[29] similar to the relative age of macaques above with a 3:1 ratio.

Decay Speed of RNFLT Between Macaques and Humans

The retina slowly loses neurons during normal aging, which is indicated by the decay of the peripapillary RNFLT in humans.[31] Similarly, the RNFLT in macaques decreased with age (Fig. 4A). In contrast with the bipolar pattern of other variables, the R^2 value of RNFLT as a function of age reached its maximum in a linear regression model (Fig. 4B), suggesting a significant linear decline in RNFLT among macaques as age increased. A similar linear decline in RNFLT with age has also been reported in human studies.[31,32] The speed of RNFLT decay in macaques was then calculated and compared with that in humans. The RNFLT in macaques displayed a negative slope of 0.70 µm/monkey year (Fig. 4B). The speed of RNFLT decay in chronologic years was strikingly faster than that in human studies (−0.16 µm/y and 95% confidence interval [−0.24 to −0.1][31] or −0.20 µm/year [−0.26 to −0.14][32]). However, taking into account the lifespan ratio of 1:3 between monkeys and humans, where one monkey year is equivalent to three years in a human's life, the negative slope of RNFLT can be converted from 0.70 µm per macaque year to 0.23 µm per human year (0.70 µm divided by 3 = 0.23 µm), which is comparable to the reported speed of RNFLT change in humans. Taken together, although the growth rate of macaques and human eyes was comparable in chronologic age with a ratio of ∼1:1, the aging of macaque eyes was faster than that of human eyes in chronologic age but not substantially different in relative age at a ratio of 3:1.

Discussion

We provided continuous reference values of the ocular biometric variables for the entire lifespan of crab-eating macaques and intensively assessed manifold age-related metrics from the aspect of ocular components between crab-eating macaques and humans. Our results suggest that they share a conserved age-related growth pattern but different growth and decline rates. The different paces between the two primates indicate that caution needs to be taken when interpreting observations from the NHP models, and further research is needed to elucidate the mechanism of age-related changes in diverse visual functions.

Age-specific ocular biometry in postnatal macaques was reported in several previous studies, most of which examined animal groups with limited age ranges or applied simple linear regression models.[7–11] In the current study, we included nearly the full range of postnatal stages with a large number of macaques. Additionally, we first introduced the IOLMaster 700, which enabled us to view the lens in vivo in macaques and precisely quantify lens thickness and density at a high resolution. With multiple regression models to explore the age-specific patterns, we discovered significant, biphasic age-specific profiles and defined the growth milestones of the major refractive components in the macaque eye. Unlike the constant spherical shape of the lens in many species, such as fish and rodents, throughout life, the shape of the human lens changes from being nearly spherical at birth to ellipsoid in adulthood.[15] This reshaping is a result of the remarkable decrease in lens thickness in the first 10 years of life.[16,17] We clearly showed that the lens thickness in macaques first decreased and then increased, which matches the age-related growth pattern of human lens and explains how the primate-specific elliptical lens in macaques develops.

Sexual maturation begins at three to five years of age in macaques and at nine to 16 years in humans, which are comparable in relative age according to the lifespan ratio.[13] In contrast, we found that during growth in both species, the turning age for lens thinning and anterior chamber deepening seemed similar at approximately 10 years. Thus the rate of lens reshaping is inconsistent with the global growth tempo between the two species, indicating that local regulation plays a role. The thinning of the human lens during childhood and puberty appears to reflect remodeling and compaction of fiber cells in the lens interior.[33] Although the precise mechanism of cellular compaction is elusive, the net effect is known to extract water from the cytosol.[15] This process may depend more on the physics of the inner contents but not global growth signals and thus requires a certain chronological time. Lens thinning can increase ACD. Notably, we found that the ACD in adult macaque eyes was relatively deeper (Table 2). The relatively longer-lasting lens thinning may partially explain the relatively deeper ACD in adult macaques. Several studies used macaques at the age of two to five years, which were equivalent to adolescent children by a lifespan ratio of 1:3, to mimic myopic progress among children in school years.[34,35] Our data suggest that during refractive eye maturation, macaques displayed a similar growth tempo to humans in chronological age at a ratio of ∼1:1. When developing a myopia model, therefore, chronological age should be appropriate.

Although the growth rates between macaques and humans were more comparable in chronological age, the alignment of the decline process appeared to differ. For aging rates, this refers to the declining trends of age-related changes, including the age of onset when the lens density starts to increase, and the decreasing speed of RNFLT over time. As individuals age, the increased protein oxidation and insolubility in the lens causes light scattering and promotes cataract formation, described as opacification.[36] The increased signal in the lens quantified from ss-OCT images reflects lens opacification during aging. The correlation of lens density with age was highest among the variables we measured, which indicates that lens density can be used

as a robust indicator of aging. The decay of RNFLT reflects age-related neural degeneration.[37] The RNFLT in macaque eyes was measured according to a standard scanning protocol by OCT in humans,[37] thus allowing meaningful comparisons. The onset of the density of lens increment and the speed of RNFLT decline were all much faster than those in humans in chronological age but similar in relative age. Thus it is reasonable to believe that aging of macaque eyes aligns well with human eyes in relative age by a ratio of ∼ 3:1. Global factors, such as nutrition, oxidative damage, and the epigenetic clock, coordinate the aging process among different tissues and determine longevity.[38–40] The close alignment of the aging process between macaque and human eyes in the relative lifespan ratio provides evidence of global but not tissue-specific factors in controlling the aging process of primate eyes. Conversely, a faster decline in macaque eyes in chronological time was illustrated, thus indicating important advantages associated with the use of macaques to examine mechanisms and therapies of human age-related eye diseases in a relatively affordable time window.

An important question is whether the decreasing trend observed in ACD, IOP, VCD, and AL in the U-shaped best-fitted lines represents a biological aging process. The decrease in ACD may be associated with lens thickening, as the rate of ACD decreases closely matches the rate of LT increase. This decrease has been consistently observed in humans.[41] Similarly, an inverted U-shaped trend between age and IOP has been observed in a large cross-sectional study of humans.[42] Recent findings from a longitudinal Large-Scale Health Examination Cohort also reported a decrease in IOP with older age in humans.[43] The consistency between our study in macaques and these human studies suggests that the U-shape of ACD and IOP are conserved in primates. Another intriguing question is whether the decrease in AL and VCD indicates a biological process that leads to eye shortening later in life. Notably, several previous studies conducted with human age cohorts have also reported progressive shortening of AL in old age (>60 years).[41,44,45] Interpreting these changes in both human and macaque studies is complex and may sometimes reflect age-period cohort effects, commonly referred to as "generation effects." For instance, key differences in secular height and educational levels exist between different age cohorts in humans. In the case of macaques, we could speculate that potentially important age-period cohort effects may be related to differences in nutrition between old and young macaques. Therefore the U-shape curve approximations may not fully align with biological processes. However, the similarity in the decreasing trends observed between macaques and humans suggests that they may represent an actual biological aging process over time.

It should be noted that the regression efficiency of the U-shape pattern in this study could be affected by the size and distribution of the cohort. The study of larger cohorts of macaques, especially at geriatric stages, would improve the ability to better recapitulate the dynamics of ocular biometry that occur in individual animals over their lifetime. A more definitive approach would be a longitudinal study of macaques over an extended period. Considering the 1:3 ratio of macaque years to human years and the potential accelerated decrease in AL in old macaques, it would be advantageous in future research to explore the biological effects of aging through longitudinal studies of old macaques (>20 years old), which might require a shorter observation time compared to human studies.

Acknowledgments

The authors thank Huazhen Biotechnology Co., Ltd, Guangzhou, China for providing the animals for examination and assisting in the sedation and care of the animals.

Supported by the National Key R&D Program of China (2018YFA0108300), the National Natural Science Foundation of China (82101329) and Guangdong Provincial Key Area R&D Program (2023B1111050004).

Disclosure: **Y. Xue,** None; **Y. Cao,** None; **S. Fan,** None; **M. Xu,** None; **Z. Yang,** None; **L. Zhou,** None; **L. Shi,** None; **L. Ou,** None; **Y. Li,** None; **W. Qing,** None; **Z. Zou,** None; **F. Mao,** None; **N. Wang,** None; **E.J. Duh,** None; **W. Yi,** None; **X. Liu,** None

References

1. Niccoli T, Partridge L. Ageing as a risk factor for disease. *Curr Biol*. 2012;22:R741–R752.
2. Iribarren R. Crystalline lens and refractive development. *Prog Retin Eye Res*. 2015;47:86–106.
3. Steinmetz JD, Bourne RR, Briant PS, et al. Causes of blindness and vision impairment in 2020 and trends over 30 years, and prevalence of avoidable blindness in relation to VISION 2020: the Right to Sight: an analysis for the Global Burden of Disease Study. *Lancet Glob Health*. 2021;9:e144–e160.
4. Mustari MJ. Nonhuman primate studies to advance vision science and prevent blindness. *ILAR J*. 2017;58:216–225.
5. Bringmann A, Syrbe S, Görner K, et al. The primate fovea: structure, function and development. *Prog Retin Eye Res*. 2018;66:49–84.
6. Chen L, Zhao Y, Zhang H. Comparative anatomy of the trabecular meshwork, the optic nerve head and the inner retina in rodent and primate models used for glaucoma research. *Vision*. 2016;1:4.
7. Lin KH, Tran T, Kim S, et al. Age-related changes in the rhesus macaque eye. *Exp Eye Res*. 2021;212:108754.
8. Augusteyn RC, Maceo Heilman B, Ho A, Parel J-M. Nonhuman primate ocular biometry. *Invest Ophthalmol Vis Sci*. 2016;57:105–114.
9. Lin KH, Tran T, Kim S, et al. Advanced retinal imaging and ocular parameters of the rhesus macaque eye. *Transl Vis Sci Technol*. 2021;10:7.
10. Choi KE, Anh VTQ, Yun C, et al. Normative data of ocular biometry, optical coherence tomography, and electrophysiology conducted for cynomolgus macaque monkeys. *Transl Vis Sci Technol*. 2021;10:14.
11. Fernandes A, Bradley DV, Tigges M, Tigges J, Herndon JG. Ocular measurements throughout the adult life span of rhesus monkeys. *Invest Ophthalmol Vis Sci*. 2003;44:2373–2380.
12. Lemaître J-F, Garratt M, Gaillard J-M. Going beyond lifespan in comparative biology of aging. *Adv Geriatr Med Res*. 2020;2:e200011.
13. Roth GS, Mattison JA, Ottinger MA, Chachich ME, Lane MA, Ingram DK. Aging in rhesus monkeys: relevance to human health interventions. *Science*. 2004;305:1423–1426.
14. Rando TA, Wyss-Coray T. Asynchronous, contagious and digital aging. *Nat Aging*. 2021;1:29–35.
15. Bassnett S, Šikić H. The lens growth process. *Progr Retin Eye Res*. 2017;60:181–200.
16. Zadnik K, Mutti DO, Fusaro RE, Adams AJ. Longitudinal evidence of crystalline lens thinning in children. *Invest Ophthalmol Vis Sci*. 1995;36:1581–1587.
17. Mutti DO, Zadnik K, Fusaro RE, Friedman NE, Sholtz RI, Adams AJ. Optical and structural development of the

crystalline lens in childhood. *Invest Ophthalmol Vis Sci*. 1998;39:120–133.
18. Hashemi H, Pakzad R, Yekta A, et al. Global and regional prevalence of age-related cataract: a comprehensive systematic review and meta-analysis. *Eye*. 2020;34:1357–1370.
19. Zeng H, Zhu W, Tan Y, Liu Z. Editorial: advances in ocular imaging and biometry. *Front Med*. 2022;9:1036038.
20. Akman A, Asena L, Güngör SG. Evaluation and comparison of the new swept source OCT-based IOLMaster 700 with the IOLMaster 500. *Br J Ophthalmol*. 2016;100:1201–1205.
21. Flaxel CJ, Adelman RA, Bailey ST, et al. Age-related macular degeneration preferred practice pattern. *Ophthalmology*. 2020;127:P1–P65.
22. Santosa Y, Kusmardiastuti K, Kartono AP, Rahman DA. Determination of long-tailed macaque's (Macaca fascicularis) harvesting quotas based on demographic parameters. 2012:13(2).
23. Simmons HA. Age-associated pathology in rhesus macaques (Macaca mulatta). *Vet Pathol*. 2016;53:399–416.
24. Rüfer F, Schröder A, Klettner A, Frimpong-Boateng A, Roider JB, Erb C. Anterior chamber depth and iridocorneal angle in healthy White subjects: effects of age, gender and refraction. *Acta Ophthalmol*. 2010;88:885–890.
25. Wang J, He X, Xiong S, et al. Distribution of anterior chamber parameters in normal Chinese children and the associated factors. *J Glaucoma*. 2018;27:357–363.
26. Bradfield YS, Melia BM, Repka MX, et al. Central corneal thickness in children. *Arch Ophthalmol*. 2011;129:1132–1138.
27. Ma R, Liu Y, Zhang L, et al. Changes in corneal morphology with age in Asian population: a multicenter study of 30,618 cases. *Adv Ther*. 2021;38:5763–5776.
28. Ganesh D, Lin SR. Global metrics on ocular biometry: representative averages and standard deviations across ten countries from four continents. *Eye (Lond)*. 2023;37:511–515.
29. Najjar RP, Teikari P, Cornut PL, Knoblauch K, Cooper HM, Gronfier C. Heterochromatic flicker photometry for objective lens density quantification. *Invest Ophthalmol Vis Sci*. 2016;57:1063–1071.
30. Kaufman PL, Bito LZ. The occurrence of senile cataracts, ocular hypertension and glaucoma in rhesus monkeys. *Exp Eye Res*. 1982;34:287–291.
31. Parikh RS, Parikh SR, Sekhar GC, Prabakaran S, Babu JG, Thomas R. Normal age-related decay of retinal nerve fiber layer thickness. *Ophthalmology*. 2007;114:921–926.
32. Chauhan BC, Vianna JR, Sharpe GP, et al. Differential effects of aging in the macular retinal layers, neuroretinal rim, and peripapillary retinal nerve fiber layer. *Ophthalmology*. 2020;127:177–185.
33. Augusteyn RC. On the contribution of the nucleus and cortex to human lens shape and size. *Clin Exp Optom*. 2018;101:64–68.
34. Smith EL, Bradley DV, Fernandes A, Boothe RG. Form deprivation myopia in adolescent monkeys. *Optom Vis Sci*. 1999;76:428–432.
35. Zhong X, Ge J, Nie H, Smith EL. Compensation for experimentally induced hyperopic anisometropia in adolescent monkeys. *Invest Ophthalmol Vis Sci*. 2004;45:3373–3379.
36. Michael R, Bron AJ. The ageing lens and cataract: a model of normal and pathological ageing. *Philos Trans R Soc Lond B Biol Sci*. 2011;366:1278–1292.
37. Tatham AJ, Medeiros FA. Detecting structural progression in glaucoma with optical coherence tomography. *Ophthalmology*. 2017;124:S57–S65.
38. Longo VD, Anderson RM. Nutrition, longevity and disease: from molecular mechanisms to interventions. *Cell*. 2022;185:1455–1470.
39. Seale K, Horvath S, Teschendorff A, Eynon N, Voisin S. Making sense of the ageing methylome. *Nat Rev Genet*. 2022;23:585–605.
40. Amorim JA, Coppotelli G, Rolo AP, Palmeira CM, Ross JM, Sinclair DA. Mitochondrial and metabolic dysfunction in ageing and age-related diseases. *Nat Rev Endocrinol*. 2022;18:243–258.
41. Fotedar R, Wang JJ, Burlutsky G, et al. Distribution of axial length and ocular biometry measured using partial coherence laser interferometry (IOL Master) in an older white population. *Ophthalmology*. 2010;117:417–423.
42. Khawaja AP, Springelkamp H, Creuzot-Garcher C, et al. Associations with intraocular pressure across Europe: The European Eye Epidemiology (E(3)) Consortium. *Eur J Epidemiol*. 2016;31:1101–1111.
43. Asaoka R, Obana A, Murata H, et al. The association between age and systemic variables and the longitudinal trend of intraocular pressure in a large-scale health examination cohort. *Invest Ophthalmol Vis Sci*. 2022;63:22.
44. Rozema JJ, Dhubhghaill SN. Age-related axial length changes in adults: a review. *Ophthalmic Physiol Opt*. 2020;40:710–717.
45. Lei Q, Tu H, Feng X, Ortega-Usobiaga J, Cao D, Wang Y. Distribution of ocular biometric parameters and optimal model of anterior chamber depth regression in 28,709 adult cataract patients in China using swept-source optical biometry. *BMC Ophthalmol*. 2021;21:178.

Investigative Ophthalmology & Visual Science